J. Phys.: Condens. Matter 3 (1991) 3905–3920. Printed in the UK

Theory of defects in conducting polymers: II. Application to polyacetylene

D S Wallace†‡¶, A M Stoneham§, W Hayes†, A J Fisher†‡ and A Testa§
† Clarendon Laboratory, Parks Road, Oxford OX1 3PU, UK
‡ Theoretical Physics Division, Harwell Laboratory, Didcot, Oxon OX11 ORA, UK
§ AEA Industrial Technology, Harwell Laboratory, Didcot, Oxon OX11 0RA, UK

Received 14 November 1990

Abstract. We exploit the approach of a previous paper, based on self-consistent quantum-chemical molecular dynamics, to investigate the energetics and dynamics of excitations in conducting polymers. The predictions include the formation energies of solitons and polarons, the phenomenon of doping by alkali atoms, luminescence quenching in *cis*-polyacetylene, the soliton mobility in *trans*-polyacetylene and the non-existence of breathers in *cis*-polyacetylene.

1. Introduction

In the previous paper (hereinafter called paper I) we outlined the development of computational techniques which can be readily used to calculate, for example, the equilibrium geometries, dipole moments and frequencies of vibration of small molecules. Here we extend the techniques to model properties, and especially defect properties, of conducting polymers like polyacetylene (PA). These conjugated polymers are semiconductors with gaps in the range 1–3 eV, but may be doped chemically and reversibly to give conductivities of up to metallic values (see e.g. Hayes 1985). At low dopant levels, conductivity appears to be due to the movement of charged defects along polymer chains but, at higher doping levels, more complicated mechanisms (e.g. hopping between chains) may occur (Kivelson 1986).

Much of the theoretical study of conjugated polymers in the past has been based on the model Hamiltonian of Su, Schrieffer and Heeger (the so-called SSH model; Su *et al* 1980) and its continuum approximation due to Takayama *et al* (1980); for a review see Heeger *et al* (1988). The SSH approach is based on extended Hückel theory and is a tight-binding model with electron–phonon, but not electron–electron, interactions; it is a relatively simple approach that has provided a framework to which later calculations could be related. The key feature of our present approach is the simultaneous optimization of molecular geometry and the self-consistent calculation of molecular electronic structure. The same approach can be readily exploited for both static and dynamical studies. In our studies of the electronic behaviour and the molecular geometry of polymers we have carried out self-consistent numerical calculations using the SSH Hamiltonian as well as both the CNDO (complete neglect of differential overlap)

¶ Present address: Andersen Consulting, 2 Arundel Street, London WC2R 3LT, UK.

0953-8984/91/223905+16$03.50

and INDO (intermediate neglect of differential overlap) parametrizations of Hartree–Fock theory. Other authors such as Stafstrom and Bredas (1988) use the MNDO (modified neglect of differential overlap) parametrization, which retains some of two-centre intregals neglected by CNDO and INDO. Sadlej (1985) has discussed all three methods.

Our method relaxes a molecule by a molecular dynamical technique, and thus requires no second derivatives to be calculated; the first derivatives are calculated analytically rather than numerically. The wavefunction calculation (which involves the recursive diagonalization of an $N \times N$ matrix, where N is the number of basis orbitals used) is the time-limiting step of the calculation, except for very small systems, and is performed in parallel with the molecular geometry calculation so that just a few steps (typically one) of the recursion is performed at each molecular geometry encountered along the minimization path. The concept of simultaneous geometry optimization and self-consistent electronic structure determination has been pioneered by Car and Parrinello (1985).

There are two further advantages to the method of geometry optimization. Since the method has a dynamical basis it can be used to obtain approximate dynamics merely by refraining from damping out the atomic motion, subject to the limitations discussed in appendix 2 of the previous paper. In particular, there is no need to calculate any second derivatives (which is an intractable process analytically; the calculation of analytic first derivatives is only made possible by the Hellman–Feynman theorem, which enables us to ignore the derivatives of the bond-order matrix). It should be noted, though, that the specific semi-empirical methods used here (INDO, and in particular CNDO) tend to overpredict force constants by a factor of approximately 2 to 3, so that calculated frequencies will tend to be too high by around 50–70%. Fortunately, this overprediction is so regular as to be almost systematic (see the previous paper). The additional advantage inherent in this method of molecular relaxation is its flexibility. Indeed, the underlying computer program has been written with this flexibility in mind. External fields (both electric and force fields) can be applied (and they need not be uniform), external potentials representing substrates may be included, and individual atoms may be constrained to remain fixed with respect to motion along any axis. There is, of course, no need to impose symmetry, nor any supposed bonding pattern.

We shall describe the structures of defects in conducting polymers in section 2 and also discuss the calculation of their energies of formation. Since doping is a key component of many proposed applications, we examine its main features in section 3. We shall also be concerned with the dynamics of defects in conducting polymers, but at the outset we look briefly at vibrations to see how effectively our quantum-chemical approach deals with effects of electron–phonon coupling. For the polyacetylenes we calculated the frequencies of Raman-active LO phonons by setting up molecules of t-$C_{24}H_{26}$ and c-$C_{32}H_{34}$ in states corresponding to excitations of LO modes. The frequencies calculated using the methods outlined in paper I, section 8.4, are 2660 cm^{-1} for t-PA and 2680 cm^{-1} for c-PA (for reasons of economy of computer time these values are precise to only about 30 cm^{-1}). These values should be scaled down by a factor of 1.7–1.8 to take account of systematic overpediction by CNDO (section 8.4, paper I), giving about 1520 cm^{-1} for t-PA (experiment 1470 cm^{-1}) and 1530 cm^{-1} for c-PA (experiment 1540 cm^{-1}). Bearing in mind the approximate nature of the compensation process, our method gives useful qualitative (or even semi-quantitative) estimates.

The calculation of frequencies and energy surfaces is central to issues of non-radiative transitions and luminescence quenching, and we discuss these matters for PA in section 4. In section 5 the dynamical behaviour of PA is modelled in order to study three effects. First, we shall examine the way in which the injection of a soliton at the end of a *t*-PA chain results in the defect moving into the chain interior. Second, we shall estimate the mobility of a charged soliton in *t*-PA. Third, we shall analyse the much-studied case of the creation of an electron–hole pair, considering the behaviour of the lowest triplet state of each isomer of PA. The behaviour of *t*-PA on photoexcitation, and in particular its dynamical behaviour, has aroused much interest because of the possibility of formation of a form of dynamical defect known as a breather (Bishop *et al* 1984), which has been postulated as the species responsible for the 1.35 eV peak in the photoinduced absorption spectrum of *t*-PA. Previous studies have used methods based on extended Hückel theory, including the SSH model, to predict the possible existence of no fewer than three types of breather, each of which may be formed if the energy injected into the system is appropriate (Wang and Martino 1986). The possibility of the existence of breathers in *c*-PA has not previously been studied, possibly because of the absence of a satisfactory model. The dynamical nature of the code used here, however, coupled with its flexibility and its high speed of calculation, means that it is ideally suited to investigations of this type (section 6).

2. Defect formation energies in conjugated polymers

Trans-polyacetylene (*t*-PA) (figure 1) has received more attention than any other conjugated polymer. The carbon atoms in the chain are s–p hybridized; if we take the plane of the polymer to be the xy plane there is one $p_z(\pi)$ electron per carbon not included in the σ-bond backbone and, in Hückel theory, the π electrons form a half-filled band. However, *t*-PA does not behave as a one-dimensional metal because of the Peierls (1951) instability, which causes a doubling of the size of the unit cell and generates a gap in the π band This dimerization was first proposed for *t*-PA by Longuet-Higgins and Salem (1959); in chemical terms, the backbone consists of alternating single and double bonds. However, the use of the terms 'single' and 'double' bond in this context is descriptive rather than precise, since the difference in bond length and bond order is not large. When considering distortion around a defect in a polymer chain it is useful to define a dimerization parameter d_n by

$$d_n = (-l)^n (b_{n,n+l} - b_{n-1,n}) \tag{1}$$

where $b_{n,n+1}$ is the length of the bond joining carbon atoms n and $n+1$. The basic defect in *t*-PA may be imagined as a junction between states (*a*) and (*b*) of figure 1; here the switch from state (*a*) to state (*b*) is imagined to be abrupt and there is an unpaired electron localized in the central carbon atom. However, in fact, the change of dimerization pattern is more extended and, in the TLM approximation is proportional to $\tanh(x/l)$ where the half-width l is about seven C–C spacings. This defect has one localized state, which is at midgap in the Hückel approximation (figure 1(*d*)); it is known as a bond-alternation defect (Pople and Walmsley 1962) or soliton (Su *et al* 1980).

Other conducting polymers, such as *c*-PA, polypyrrole and polythiophene do not have the topological degeneracy typical of *t*-PA (figure 1), and hence a soliton is

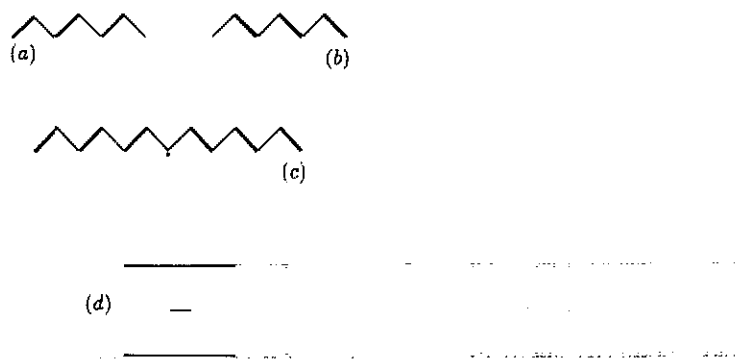

Figure 1. Topological representation of a soliton in *t*-PA; the defect (state (*c*)) consists of a change in the backbone of the chain from state (*a*) to state (*b*) and gives rise to a localized electronic state at the centre of the gap (see (*d*)).

not possible. The only simple defect that can occur in non-degenerate polymers is represented by a reduction of the dimerization parameter over a limited region of chain. A possible structure for *c*-PA is represented in figure 2(*a*). This type of defect is associated with two localized electronic states which, within the SSH approximation, are symmetrically located about midgap (figure 2(*b*)); it is not stable in an uncharged state, and will decay immediately into the ground state. However, the addition of a single charge will stabilize the defect, forming a polaron. One may envisage addition of a second charge; if the doubly charged defect were stable against decay into two polarons we would have a negative U effect and formation of a bipolaron. The localized electronic states of a bipolaron (figure 2) resemble those of a polaron, but are expected to be closer to the centre of the gap because of greater chain distortion.

Figure 2. (*a*) Topological representation of a polaron in *c*-PA with (*b*) its two localized electronic states in the gap.

The spin–charge relations of a soliton are unusual. In a neutral chain, the soliton is associated with an unpaired electron, and has $S = 1/2$. This unpaired electron can be removed, or another added, giving solitons with spin $S = 0$ and charge $\pm e$. A defect-free chain with an even number of carbon atoms is terminated by a 'double' bond at each end; if we attempt to create a single soliton, one end of the chain is forced to end with a 'single' bond, thereby leading to a second unpaired electron. We conclude that localized defects cannot be created singly in an even length chain. A uniformly dimerized chain with an odd number of carbons and no defects is forced to end with a 'single' bond and an unpaired electron. The state associated with this unpaired spin is free to move on up the chain, but cannot vanish, and so a chain with

an odd number of carbons must have a single localized defect.

The calculation of the energy of formation of the defects mentioned above has recently been investigated by Wallace (1989) (see also Fisher *et al* 1989) and some results are given here. The calculations involve the self-consistent solution of the SSH Hamiltonian, with an extra term added to model non-degenerate polymers such as *c*-PA; the electronic part of the Hamiltonian is diagonalized for given atomic displacements and then the atoms are relaxed to make the force acting on each one zero (Wallace 1989, section 2.2). Use of SSH theory for *t*-PA gives a formation energy E_F of 0.56 eV for charged solitons and 0.34 eV for uncharged solitons; by contrast the calculated E_F for a polaron is 0.63 eV, suggesting that in *t*-PA solitons are preferentially formed. CNDO predicts somewhat greater values, but reaches the same conclusions. The SSH value for E_F for a polaron in *c*-PA is 0.89 eV, and again CNDO predicts a slightly greater lattice distortion. Presumably this is in part because it takes into account repulsion of the charged carbon atoms and so tends to spread the defect out further.

For *t*-PA both SSH and CNDO agree that the bipolaron is unstable with respect to decay into two charged solitons. We cannot calculate the energy of a bipolaron since the geometry relaxation routines lead to a decay into solitons. In *c*-PA the two-soliton route for bipolaron break-up is forbidden and within SSH the energy required to form a bipolaron is 1.51 eV i.e. 0.27 eV less than the calculated formation energy of $2 \times 0.89 = 1.78$ eV (see above) for two separate polarons. It is not surprising that bipolarons are predicted to be stable in the SSH model, since the electron–electron interaction is ignored. We shall discuss the corresponding predictions of CNDO in a subsequent publication.

3. Doping by alkali atoms

The important properties of *t*-PA are controlled by doping, for example by Na. This process is hard to treat realistically in the SSH or similar models; usually the dopant is supposed merely to donate a charge to the polymer, though Bryant and Glick (1982) did give a simple phenomenological treatment of the distortion due to the dopant. Our approach allows us to handle the charge transfer and deformation consistently, and casts doubt on the usual assumptions.

We show in figure 3 the equilibrium positions resulting when a Na atom is placed close to a t-$C_{24}H_{25}$ chain. This is still a relatively simple case, but it shows features relevant to a bulk system. The Na atom moves from an initial asymmetric position to a stable minimum out of the molecular plane and midway between two carbons. The in-plane distortion of the chain has the major effect on the π electron coupling and dimerization. Close examination of the deformation shows two components: one has the shallow but broad distortion of a polaron; the other is a localized term associated with short-range overlap interactions. Not only is the deformation pattern more complex than often supposed, but also the charge transfer is less complete: for Na dopant, the (Mulliken) charge stored in the chain is only 0.71*e*. For smaller ions like Li and F, less than 0.3*e* transfer is predicted.

4. Luminescence quenching in *c*-PA

The spectrum of scattered light from photoexcited *c*-PA consists of a broad luminescence peak centred at 1.9 eV, with a multiple overtone Raman spectrum

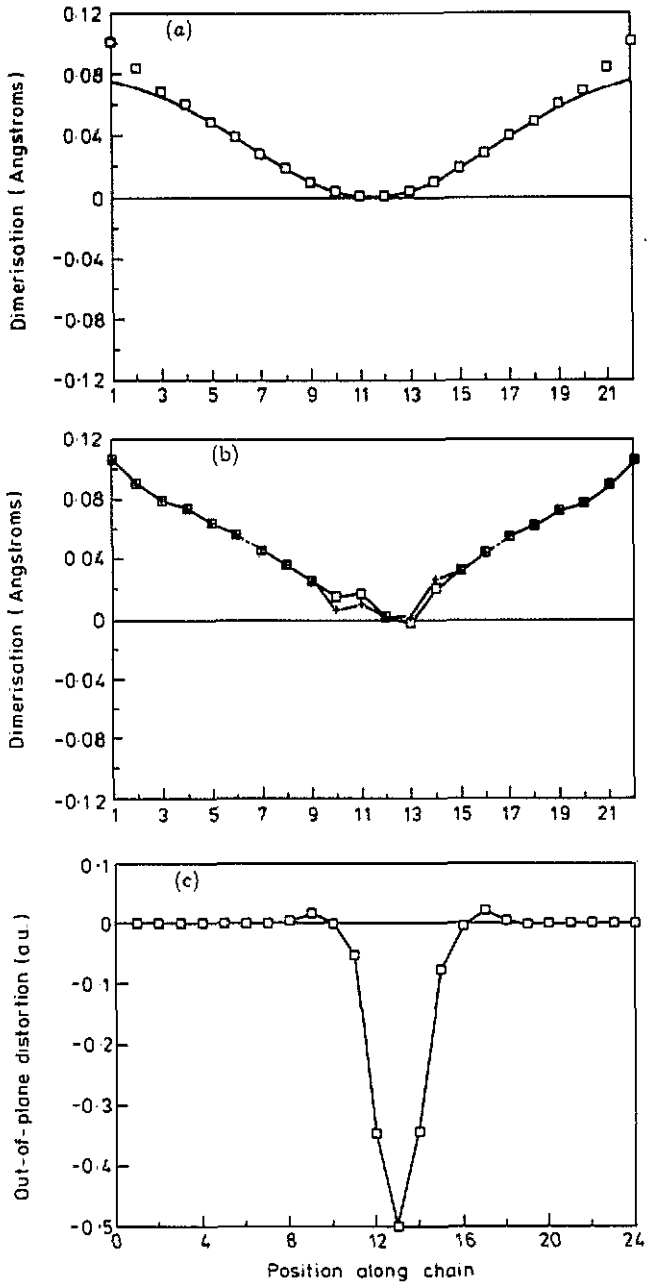

Figure 3. (*a*) Dimerization pattern for a polaron in *t*-PA. The full curve is a fit to the sum of two tanh functions, of width 5.1 and separation 9.4 C–C bond lengths; this is the form predicted for a polaron in the SSH model. (*b*) Dimerization pattern induced in t-PA by the presence of a nearby Na atom ≈ 2.5 Å from the chain. + correspond to a dimerization parameter calculated from the actual bond lengths; □ refer only to the component of the distortion in the plane of the molecule. The overall effect is similar to the polaron shown in (*a*) but with the addition of short-range distortion near the Na atom. The plot is slightly asymmetric because relaxation is not complete. (*c*) Out-of-plane component of the distortion of a t-PA chain produced by doping with a Na atom, as in (*b*).

superimposed (Lauchlan *et al* 1981). The luminescence requires an excitation energy of 2.05 eV, and has a low quantum efficiency of at most 10^{-5}. Hayes *et al* (1983) concluded that the luminescence lifetime was shorter than 9 ps and suggested that hot luminescence was involved. Tubino *et al* (1984) suggested that the apparent Stokes shift of 0.15 eV was, in fact, due to a shallow gap state (see also Andrews *et al* 1989).

Shank *et al* (1982) studied the time dependence of a photoinduced absorption peak of *c*-PA at 1.6 eV. They found that the absorption consisted of two components: one short-lived, with a decay time of order picoseconds, and one long-lived, with a lifetime of at least some milliseconds. The frequency profiles of these two components were identical, implying that they arose from the same source, and their intensities were comparable, with the short-lived component having roughly double the strength of the long-lived component. The absorption appeared to start immediately upon excitation, implying a formation time for the species responsible of less than 150 fs.

One of the shortfalls of the SSH model is its failure to account for the low quantum yield of photoluminescence in *c*-PA (Hayes *et al* 1983, Andrews *et al* 1983). The SSH model Hamiltonian displays charge-conjugation symmetry (CCS) which forbids non-radiative decay from a photoexcited state to the ground state (Danielsen and Ball 1985); there is the possibility that the low efficiency of luminescence is due to a competing non-radiative transition, in violation of this artificial symmetry (Hayes 1985), and various authors (Su *et al* 1988, Danielsen and Ball 1985) have suggested possible mechanisms for this symmetry breaking. The use of CNDO in place of SSH automatically breaks the symmetry. We have verified this explicitly by calculations of optical absorption weights (Wallace 1989). The photoluminescence of *c*-PA is still an area worthy of study, however, since it will become clear below that straightforward competition from a non-radiative decay mode will not explain all of the observed features.

The Huang–Rhys factor for an electronic defect in *c*-PA has a value which depends on the shape of the distortion pattern as well as on its amplitude. However, the dependence on the defect shape (dimerization pattern) is fairly weak (Wallace 1989), so to a first approximation the amplitude can be treated as the most important parameter. We define this amplitude by a 'depth' α, the ratio of the maximum change in the dimerization parameter to its ground-state value d_0:

$$\alpha = \frac{|d_n - d_0|_{\max}}{d_0}. \tag{2}$$

Typical values for the parameters which define the defect shape give a Huang–Rhys factor of $S_0 \approx 2\alpha^2$ (Wallace 1989). Values of α can be found by self-consistent geometry optimization in either the SSH or semi-empirical Hartree–Fock models and, for an exciton in *c*-PA, these methods lead to values of 1.05 and 1.8 respectively. Since the Stokes shift is equal to $2S_0\hbar\omega$, and the phonon energy $\hbar\omega$ is 0.18 eV in *c*-PA (Lefrant *et al* 1979), it is clear that, if the apparent Stokes shift of 0.15 eV is genuine, there is a discrepancy between theory and experiment of about an order of magnitude.

It can be confirmed that this discrepancy is not due to any of the approximations involved in calculating the Huang–Rhys factor by looking at the results of explicit calculations of the energies of various defects within the SSH model. The energy saved by lattice relaxation around a polaron in *c*-PA is 0.08 eV, in good agreement with the calculated value of α of 0.4. For a bipolaron, which is equivalent to an exciton in the SSH model (by charge conjugation symmetry), the equivalent energy is 0.45 eV, again in good agreement with the calculated defect depth of 1.05.

Within any self-consistent electronic structure calculation, including CNDO, constraining a system to remain in an excited state is not easy. The difficulties occur whenever there is a lower-energy state of the same symmetry to the one under consideration. One way round this problem is to consider an excited state with different spin, and our calculations for an exciton were performed on its triplet state. The accuracy of the calculations for the singlet state reached optically rely on the energy splitting between equivalent (excited) singlet and triplet states not being too great. Relative to the ground-state energy the following values were obtained:

Triplet energy at ground-state geometry = 3.67 eV.
Triplet energy (relaxed geometry) = 1.73 eV.
Energy of 'ground state' at relaxed triplet geometry = 2.21 eV.

It can be seen that the relaxation energy of the exciton is 1.94 eV, fairly close to the lattice energy of the ground state at the relaxed excited state (exciton) geometry, consistent with vibrational mode frequencies which do not change appreciably on photoexcitation. We remark again that CNDO is primarily a method for calculating good molecular geometries, rather than good energies; it tends to overpredict energies (notably phonon energies), and the energies quoted above might be too large by a factor up to two (see paper I). Given that the phonon energies will be overpredicted, it will still be possible to predict the defect geometry correctly if the band gap (i.e. the triplet energy at the ground state geometry) is also overpredicted. This is the case here, so it is possible to have some confidence in the general features of our calculations.

Configuration co-ordinate diagrams for *c*-PA within the SSH and CNDO models are shown in figure 4. The chain energy has been plotted as a function of the defect depth α, assuming harmonicity and (for the SSH model) that there is no change in vibrational frequency on photoexcitation. With these assumptions, enough is known from calculations of the geometries and energies of the ground and excited states to enable these diagrams to be drawn. The observed Stokes shift is substantially lower than predicted theoretically from both SSH and CNDO calculations, and an explanation for this may be found in the very short lifetime of the luminescence. This would imply that the observed luminescence is actually hot luminescence, occurring before the chain has had time to reach its equilibrium geometry (see Hayes *et al* 1983 and Laughlan *et al* 1983). The possibility that luminescence quenching is due to a competing non-radiative process is found to be unsupportable within the SSH model. This is because non-radiative decay is forbidden not only by symmetry, but also because the crossover between the ground-state and excited-state energy curves occurs at significantly higher energy than the vertical excitation energy (figure 4(*a*)); there is no way that the geometry necessary for the proposed non-radiative transition to take place can ever be attained. The SSH model therefore predicts 100% luminescence, irrespective of any symmetries that may or may not forbid non-radiative decay. Clearly this result is in complete disagreement with experiment, and the reason for this discrepancy will be discussed below.

Within CNDO the energy minimum of the excited curve occurs outside the ground-state energy curve (figure 4(*b*)). Once the excited state has reached its relaxed geometry, a vertical transition to the ground state is impossible. The absence of strong luminescence is therefore immediately explained, as is the presence of the long-lived state detected in photoinduced absorption by Shank *et al* (1982). There will be

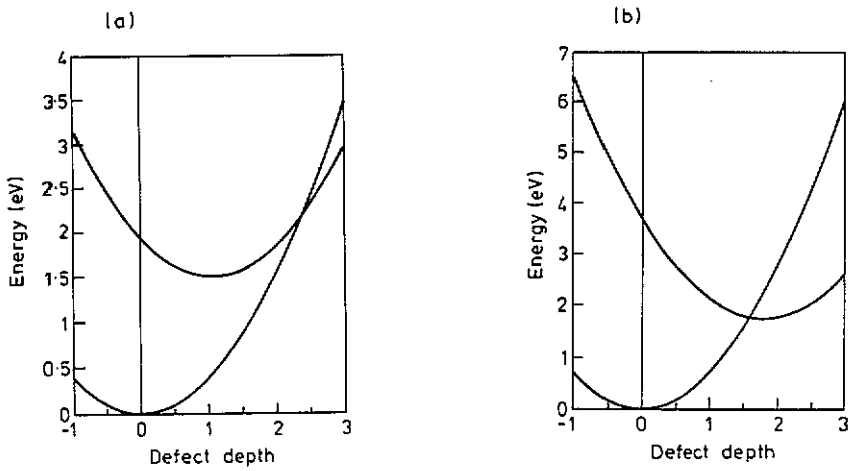

Figure 4. Calculated configuration coordinate diagrams for an exciton in c-PA using (*a*) the SSH and (*b*) the CNDO models.

a significant amount of energy in the system soon after excitation and this could raise the excitons' energy up to the cross-over thereby permitting some fast non-radiative decay and accounting for the short-lived component observed by Shank *et al* (1982). This explanation of the observed luminescence quenching does not remove the need for charge-conjugation symmetry to be violated, but does allow for the magnitude of the violation to be much smaller than that required by a simple radiative–non-radiative competition model.

The principal difference between the predictions of the SSH and CNDO models occurs because of their differences in the predicted depths of the defect, i.e. the values predicted for the configuration co-ordinate at which the excited-state energy minimum occurs. It seems that the main reason for the difficulty in reconciling experiment and the SSH predictions for *c*-PA efficiency of luminescence lies with the method by which the SSH model has been adjusted to deal with polymers without ground-state degeneracy. One of the advantages of CNDO is that it makes no comparable arbitrary assumptions.

5. Soliton velocity, sound velocity and soliton mobility in *t*-PA

Su and Schrieffer (1980) studied the effect of setting up a chain of *t*-PA with a soliton at one end. This may be done by starting with an odd-length chain and uniform dimerization, so the chain ends with a long bond and an associated localized state (see figure 1). Su and Schrieffer (1980) adjusted the parameters of the SSH model so that the defect size was reduced, thereby enabling them to use a smaller chain than otherwise necessary. They found that the soliton moved up the chain with a characteristic velocity similar to the speed of sound c in *t*-PA, which had been estimated by Guinea (1984) to be $1.85 \times 10^4 \mathrm{ms}^{-1}$ within the SSH model. Our quantum molecular dynamic method is ideally suited to the repetition of these calculations within CNDO, and the results are shown in figures 5–7.

Our first calculation (figure 5) measures the speed of sound in *t*-PA within CNDO, showing that a pulse travels down a chain of *t*-PA at a constant speed of approximately

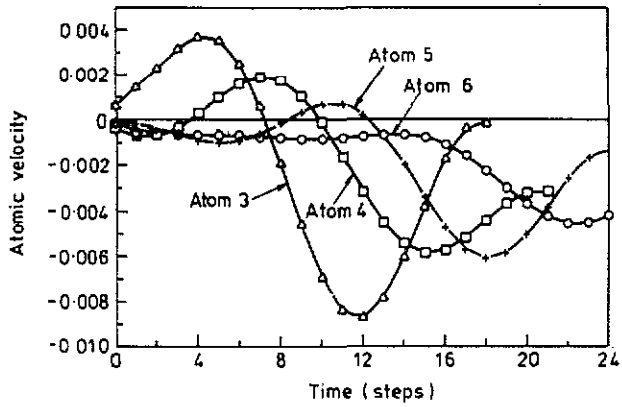

Figure 5. Determination of the speed of sound in *t*-PA from the speed at which a pulse injected at one end of the chain at $t = 0$ is calculated to move down the chain. The velocities of carbon atoms further down the chain are plotted against time (△, atom 3; □, atom 4;+, atom 5; ◇, atom 6). The pulse is attenuated as it travels.

0.3 carbon atoms per time step. The pulse was generated by reducing the lengths of the two bonds at one end of the chain by 0.05 Å and allowing the chain to relax without applying any damping. Even though there is no external damping, the pulse is significantly attenuated as it travels, presumably from dispersion (and indeed the peak positions do suggest more than one component). The time step used was the program's natural unit of time, which is $\sqrt{m_p}$ atomic units (or approximately 1.04 fs), representing a sound velocity of $c_s = 3.5 \times 10^4\,\mathrm{ms}^{-1}$. The overprediction of force constants by a factor of 1.9 is characteristic of CNDO (see paper I) and is responsible for the speed obtained being rather higher than the SSH result.

The results in figure 6 repeat the SSH calculations of Su and Schrieffer for an end-injected soliton, here using the CNDO dynamic model. The dimerization pattern is plotted at three different times. We observe that the relaxation of the defect into a soliton appears to be occurring fairly quickly; further, the speed at which the soliton moves up the chain remains constant to a good approximation. This velocity is 0.10 carbon atoms per time step, corresponding to approximately $1.2 \times 10^4\,\mathrm{ms}^{-1}$, a figure which is comparable to the speed of sound.

We emphasise that quite different motions are involved in the two cases. The sound velocity of $3.5 \times 10^4\,\mathrm{ms}^{-1}$ describes the propagation of a small deviation from equilibrium, with no bond alternation defect present. The soliton velocity of $1.2 \times 10^4\,\mathrm{ms}^{-1}$ describes the motion of a bond-alternation defect and is, in effect, the product of the soliton mobility (see below) and the effective force field arising because of the lower energy of the soliton at the chain centre.

The large size of a soliton ($l \approx 8$ carbon units) implies a low effective mass. Su *et al* (1980) calculated $M_{\mathrm{eff}} \approx 6m_e$, and hence a high mobility. Our method allows us to calculate the soliton mobility directly within the self-consistent quantum chemical model. Such a calculation uses both the model's dynamical nature and the facility it provides for the application of an external electric field. Results given in figure 6(*c*) show how the dimerization pattern of a soliton moves along a chain under the influence of an applied field of 10^{-3} au, or approximately $5 \times 10^8\,\mathrm{Vm}^{-1}$. Snapshots of the soliton position are shown at intervals of five steps (with the time step approximately 1 fs, as above), and it can be seen that the soliton's velocity remains fairly constant throughout

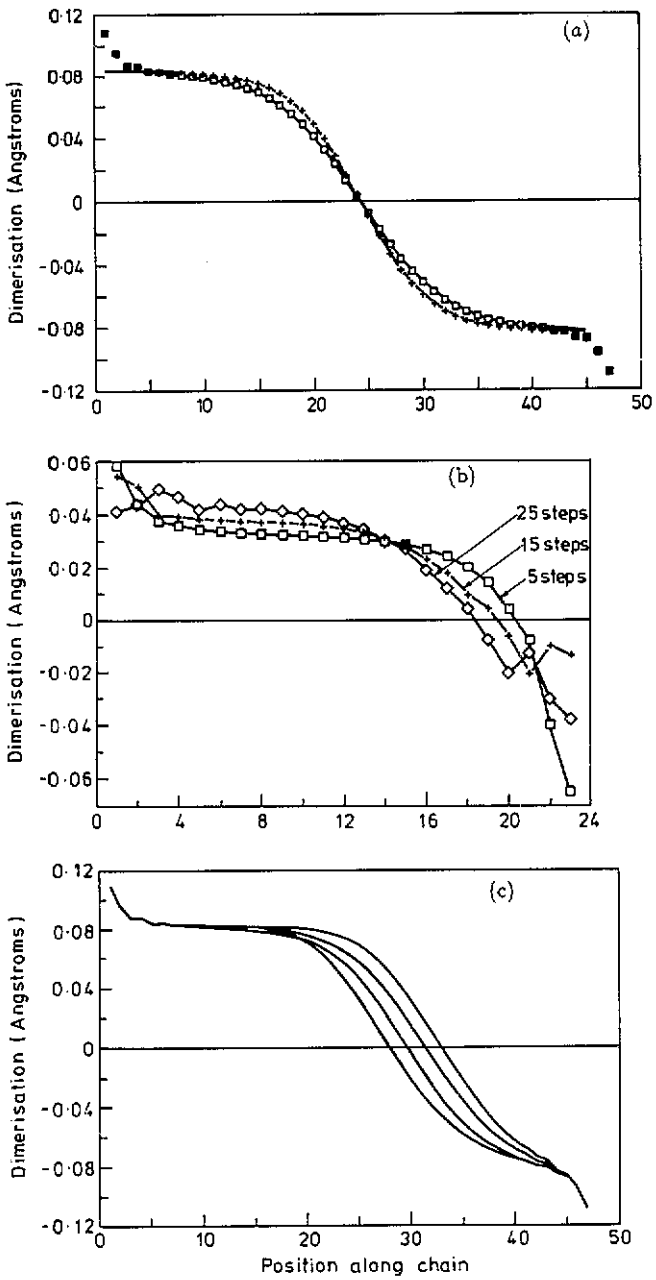

Figure 6. (*a*) Dimerization patterns for charged (□) and uncharged (+) solitons in *t*-PA. Full curves are fits to tanh curves of half-widths 8.1 and 6.5 C units for the charged and uncharged solitons respectively. (*b*) Relaxation of the dimerization parameter along an odd-length chain with time: □ after 5 time steps, + after 15 time steps, ◇ after 25 time steps. The point at which the dimerization crosses zero is moving at approximately 1.2×10^4 ms^{-1}. (*c*) Evolution with time of the dimerization parameter along a chain containing a positively charged soliton, under the influence of an electric field (see text). The curves are separated by 5 time steps. A soliton mobility of $\mu = 0.75\,\mathrm{cm^2V^{-1}s^{-1}}$ can be deduced from the velocity of the point at which the dimerization crosses zero.

the run. This velocity is measured to be $3.9 \times 10^4\,\mathrm{ms}^{-1}$, corresponding to a mobility μ of $0.75\,\mathrm{cm}^2\mathrm{V}^{-1}\mathrm{s}^{-1}$. The mobility is itself consistent with the soliton velocity estimated above where, instead of an applied electric field, the soliton moves in response to the gradient of its energy as a function of position along the chain. Experimental evidence for the soliton mobility comes from two sources: magnetic resonance experiments (Conwell and Jeyadev 1989) and picosecond studies of photoconductivity (Sinclair *et al* 1986); other sources (e.g. Burroughes *et al* 1989, Townsend *et al* 1989) measure the mobility limited by interchain hopping, which is a different phenomenon). Both of these sources yield approximately $1\,\mathrm{cm}^2\mathrm{V}^{-1}\mathrm{s}^{-1}$ for the mobility, in good agreement with the results of the model used here.

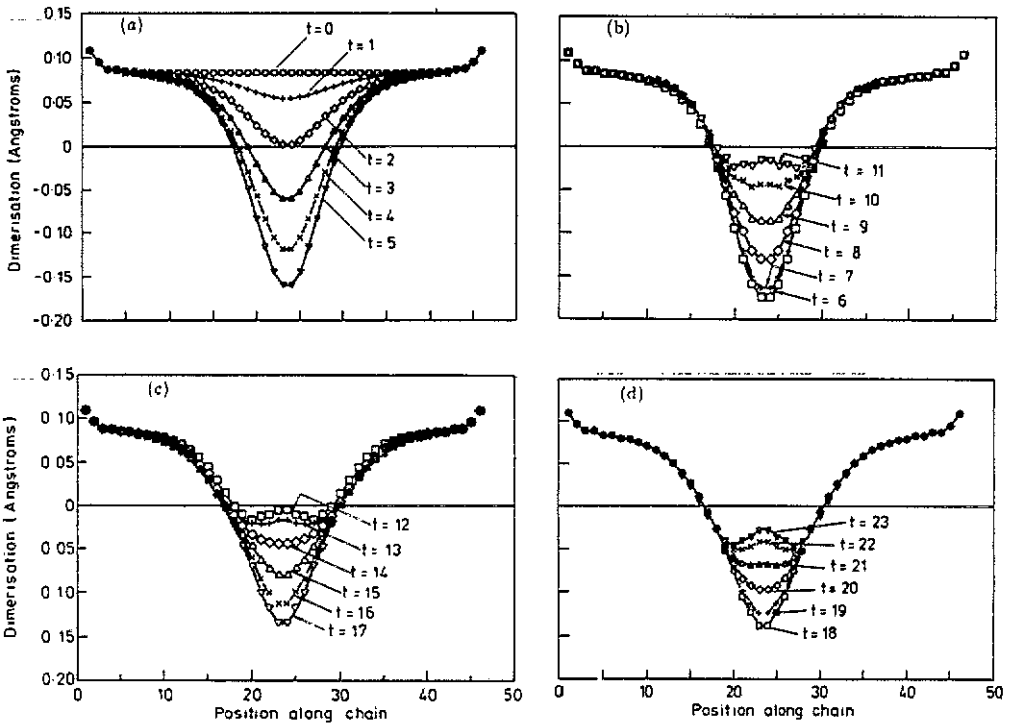

Figure 7. Illustration of breather formation in t-PA. An electron–hole pair is injected at $t = 0$ when the chain is uniformly dimerized. The dimerization that develops as a function of time represents that of a bound soliton-antisoliton pair with a local oscillation of the atoms at the centre of the defect superimposed. The dimerization is plotted in (*a*) for $t = 0$ to 5 (*b*) $t = 6$ to 11 (*c*) $t = 12$ to 17 (*d*) $t = 18$ to 23 time steps (1 time step $\approx$ 1 fs).

The dependence of the mobility on applied field both confirms our estimate and suggests an upper limit to the soliton velocity. When the calculation was repeated for a field five times smaller, a slightly larger value was obtained ($\mu \approx 0.79\,\mathrm{cm}^2\mathrm{V}^{-1}\mathrm{s}^{-1}$). This difference, if significant, does not appear to be due to the effects of localization within the chain. The soliton mobility was also calculated with electric fields two and four times as large as that applied above. The first calculation led to an approximate doubling of the soliton velocity, i.e. roughly constant mobility, but when the field was increased to 4×10^{-3} au ($2 \times 10^9\,\mathrm{Vm}^{-1}$) the soliton broke up, rather than move along

the chain as before. It therefore appears that there is a limit to the soliton velocity of about $10^5\,ms^{-1}$, i.e. a few times the speed of sound in *t*-PA. Bishop *et al* (1984) first remarked that there should be a limit to the soliton velocity, and Guinea (1984) predicted, using a modified SSH model, that this velocity would be $4.8 \times 10^4\,ms^{-1}$, larger by a factor of 2.6 than his value for the speed of sound. Such an effect is clearly carried over into our CNDO calculations. Conwell and Jeyadev (1989) have suggested that, at velocities similar to the maximum velocity, effects similar to relativistic effects might increase the soliton's effective mass and hence decrease its mobility.

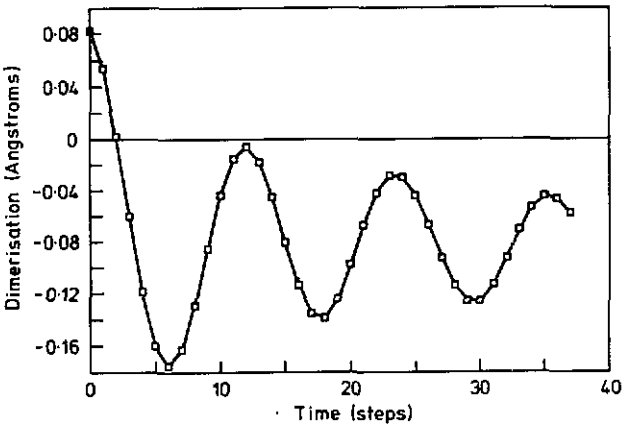

Figure 8. Dimerization at the centre of a breather in t-PA (see figure 7) plotted against time (1 time step $\approx$ 1 fs) showing the slightly damped oscillation of the bonds.

6. Amplitude breathers

Charged solitons can be created in *t*-PA by chemical doping. Photo-excitation produces an electron–hole pair which, in *t*-PA, evolves rapidly into a charged soliton–antisoliton pair. The 'mid-gap' photo-induced absorption at about 0.5 eV is then clearly similar to the 0.6-0.7 eV absorption in doped *t*-PA. However, the photo-induced absorption contains an extra transition at 1.35 eV (Grenstein and Baker 1982, Vardeny *et al* 1982, Shank *et al* 1982) which appears to be associated with a so-called 'amplitude breather' (Bishop *et al* 1984). The breather is a spatially localized charge-neutral oscillation which emerges as the solitons generated by photo-excitation move apart. If an electron at the top of the valence band is excited into the bottom of the conduction band (requiring the band gap energy Δ_0) the excitation evolves into a soliton and an antisoliton with rest energy $\approx 1.3\Delta_0$, moving apart with kinetic energy $\approx 0.2\Delta_0$. The 'breather' left behind oscillates with a frequency of about 95% of the Raman frequency. It gives rise to two electronic states within the gap; the upper one is empty, the lower is doubly occupied, and the observed 1.35 eV transition is consistent with excitation from the lower state to the upper one.

The breather decays by phonon emission, with no electronic transitions involved. An isotope effect is predicted. Consistent with this, Vardeny *et al* (1984) find the breather peak at 1.39 eV in hydrogenated *t*-PA $(CH)_n$ and 1.35 eV in deuterated *t*-PA $(CD)_n$. Further theoretical studies (Wang and Martino 1986) indicate different

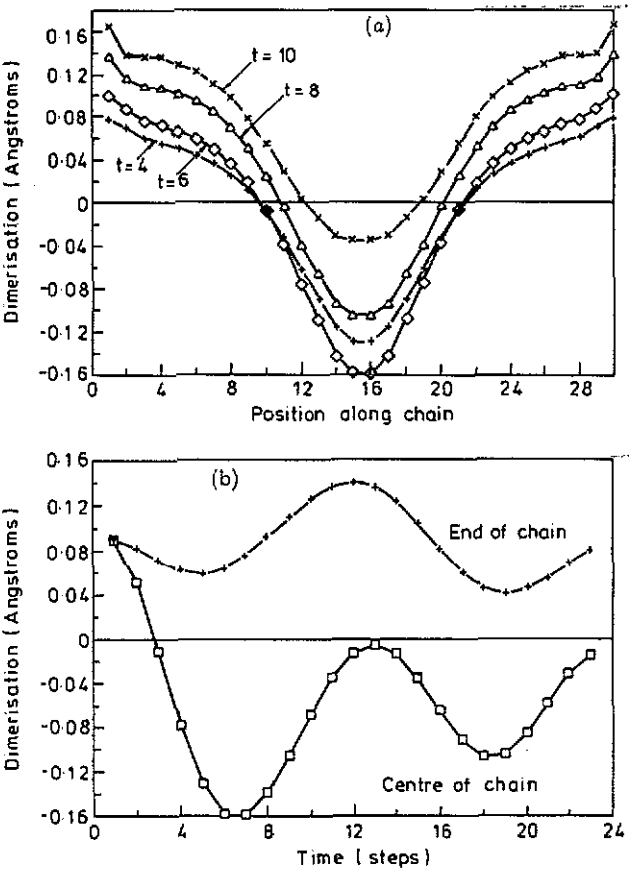

Figure 9. (*a*) Dimerization pattern in c-PA plotted as a function of time ($t = 4$ to 10 time steps) after injection of an electron–hole pair at $t = 0$ (compare figure 7 for t-PA). The oscillation that develops as a function of time represents that of a bound soliton-antisoliton pair with an oscillation of the entire chain (i.e. the LO phonon mode) superimposed. (*b*) Dimerization at the centre of the chain (squares) and near the end of the chain (crosses) plotted against time. The two dimerizations separate initially but after about 10 time steps (10^{-14} s) begin to oscillate in unison at the frequency of the LO mode.

types of breather. In a dynamical simulation using the SSH extended Hubbard model, Wang and Martino (1986) verify the conclusions of Bishop *et al* (1984), but find that if the soliton–antisoliton pair has less than a critical energy E_c they bind to give an 'excitonic breather'. The excitonic breather has an energy $1.82\Delta_0$, rather less than the value $1.88\Delta_0$ of the 'central breather'. The 'central breathers' are themselves of two types: a localized form, like that proposed by Bishop *et al* (1984), and a form which moves up and down the chain.

Our calculations on *t*-PA were based on the lowest spin-triplet state of t-$C_{48}H_{50}$ and give clear evidence for the localized form of central breather. The dynamical behaviour is shown in figure 7 and illustrates the evolution after an electron–hole pair is created in a uniformly dimerized chain. There is a clear additional oscillation of the central atoms, beyond that of the soliton–antisoliton pair. As time proceeds, the energy in the breather is slowly dissipated, at least partly because of the finite timestep

in our calculation. The motion of the atoms in the breather has a period $\tau = 12$ fs (corresponding to 2800 cm^{-1}) , which is close to that of the Raman-active LO mode (2660 cm^{-1}, see section 1), in agreement with previous theory.

The periodic motion associated with the breather is still clear at the longest times we considered, nearly 40 timesteps (figure 8). In contrast, in *c*-PA there is no stable localized oscillation: the electron–hole pair rapidly becomes an exciton plus longitudinal optic vibration of the whole chain (figure 9), consistent with the absence of a breather absorption band in this material.

Acknowledgments

DSW and AJF acknowledge the receipt of Research Studentships from the SERC and AJF thanks St John's College, Oxford, for the award of a Junior Research Fellowship. Part of this work was supported by the Underlying Research Programme of the United Kingdom Atomic Energy Authority and part by the Commission of the European Communities (contract No C11.0324).

References

Andrews J R, Orlowski T E, Gibson H, Slade M L, Knox W and Wittsmerhaus B 1983 *Phys. Rev.* B **27** 6545

Bishop A R, Campbell D K, Lomdahl P S, Horovitz B and Philpott S R 1984 *Phys. Rev. Lett.* **52** 671

Bryant G W and Glick A J 1982 *Phys. Rev.* B **26** 5855

Burroughs J H, Jones C A, Lawrence R A and Friend R H 1989 *Proc. Mons NATO Advanced Study Institute* at press

Car R and Parrinello M 1985 *Phys. Rev. Lett.* **55** 2471

Conwell E M and Jeyadev S 1989 *Synth. Met.* **28** D439

Danielsen P L and Ball R C 1985 *J. Physique* **46** 1611

Fisher A J, Hayes W and Wallace D S 1989 *J. Phys.: Condens. Matter* **1** 5567

Guinea F 1984 *Phys. Rev.* B **30** 1884

Hayes W 1985 *Contemp. Phys.* **26** 421

Hayes W, Ironside C N, Ryan J F, Steele R P and Taylor R A 1983 *J. Phys. C: Solid State Phys.* **16** L729

Hayes W and Stoneham A M 1985 *Defects and Defect Processes in Non-Metallic Solids* (New York: Wiley)

Heeger A J, Kivelson S, Schrieffer J R and Su W-P 1988 *Rev. Mod. Phys.* **60** 781

Kivelson S 1986 *Solitons* ed S E Trullinger *et al* (Amsterdam: Elsevier)

Lauchlan L, Chen S P, Etemad S, Kletter M, Heeger A J and MacDiarmid A G 1983 *Phys. Rev.* B **27** 2301

Lauchlan L, Etemad S, Chund T C, Heeger A J and MacDiarmid A G 1981 *Phys. Rev.* B **24** 3701

Lefrant S, Lichtman L S, Temkin H, Fitchen D B, Miller D C, Whitewall D E and Burlitch J M 1979 *Solid State Commun.* **29** 191

Longuet-Higgins H C and Salem L 1959 *Proc. R. Soc.* A **251** 172

Peierls R E 1955 *Quantum Theory of Solids* p 108 (Oxford: Clarendon)

Pople J A and Walmsley S H 1962 *Mol. Phys.* **5** 15

Shank C V, Yen R, Fork R L, Orenstein J and Baker G L 1982 *Phys. Rev. Lett.* **49** 1660

Sinclair M, Moses D and Heeger A J 1986 *Solid State Commun.* **59** 343

Stafström S and Brédas J L 1988 *Phys. Rev.* B **28** 4180

Su W P and Schrieffer J R 1980 *Proc. Nat. Acad. Sci.* **77** 5626

Su W P, Schrieffer J R and Heeger A J 1980 *Phys. Rev.* B **22** 2099

—— 1983 *Phys. Rev.* B **28** 1138 erratum

Takayama H, Lin-Liu Y R and Maki K 1980 *Phys. Rev.* B **21** 2388

Tubino R, Piseri L, Dellepiane, Birman J L and Pedretti U 1984 *Solid State Commun.* **49** 161
Vardeny Z, Ehrenfreund E, Brafman O, Nowak M, Schaffer H, Heeger A J and Wudl F 1986 *Phys. Rev. Lett.* **56** 671
Vardeny Z, Strait J, Moser D, Chung T C and Heeger A J 1982 *Phys. Rev. Lett.* **49** 161
Wallace D S 1989 *DPhil Thesis, Oxford University and Harwell Laboratory Theoretical Physics Division Report* TP1331
Wang C L and Martino F 1986 *Phys. Rev.* B **34** 5540